Optical and Conformational Studies on Benzobisthiazole Derivatives

Jun-Gill Kang,*,† Hyun-Joon Kim,† Yong-Kwang Jeong,† Min-Kook Nah,† Changmoon Park,† Young Ju Bae,‡ Sang Woo Lee,‡ and In Tae Kim*,‡

Department of Chemistry, Chungnam National University, Daejeon 305-764, Republic of Korea, and Department of Chemistry, Kwangwoon University, 447-1 Wolgye-Dong, Nowon-Ku, Seoul 139-701, Republic of Korea

Received: December 20, 2009; Revised Manuscript Received: February 1, 2010

2,6-Didodecyl-4,8-diphenyl-benzo[1,2-*d*;4,5-*d*′]bisthiazole (**3**) and 2,6-didodecyl-4,8-dipyrrole-2-yl-benzo[1,2-*d*;4,5-*d*′]bisthiazole (**5**) were synthesized, and their optical properties were investigated in solution and in the solid state. Compounds **3** and **5** were excited with the 325 nm He−Cd laser line to produce blue and green luminescence, respectively. The luminescence of **5** ($\Phi = 14\%$) was more efficient than that of **3** ($\Phi = 5\%$). Structural and optical properties were further determined with DFT and ZINDO calculations. The planar structure of **5** results in $\pi \rightarrow \pi^*$ electronic transitions from the pyrrole moiety to the benzobisthiazole frame, while the twisted geometry of **3** results in luminescence strongly associated with the $\pi \rightarrow \pi^*$ transitions within the benzothiazole frame. The effect of solvent on the luminescence properties of **5** is summarized as competition between intra- and intermolecular NH···N hydrogen bonds.

Introduction

Recently, benzobisthiazole derivatives have attracted great attention because of their conduction properties,[1–4] photochromic properties,[5,6] and electroluminescence properties.[7,8] However, most of the research to date has focused on the derivatives in which electron-rich groups are substituted at the 2 and 6 positions. Until now, the structural and optical properties of 4,8-disubstituted benzobisthiazole derivatives have not been reported. Recently, we reported the successful synthesis and structural and optical properties of 2,6-dihexyl-4,8-dithiophene-2-yl-benzo[1,2-*d*;4,5-*d*′]bisthiazole (**6**, Chart 1) and its copolymer.[9,10] The monomer **6**, when excited in UV, produced a blue emission when dissolved in $CHCl_3$ and a green emission from the solid state. Under the same conditions, its copolymer produced a yellow emission when dissolved in $CHCl_3$ and a red emission from a thin solid film. The large red shift in the emission from the copolymer could be due to the extension of the π-conjugation. X-ray crystallographic data of the monomer have indicated that the observed dihedral angle between the benzobisthiazole frame and the thiophene moiety was only 21°, suggesting that the crystal stacking and the electronic resonance effects were sufficient to overcome any steric hindrance: the Ortep view of **6** is given in Figure S1 (in Supporting Information). Some debate, however, exists as to the optical processes and their relationship to different structural conformations for the benzobisthiazole derivatives in which electron-rich groups are substituted at the 4 and 8 positions. To elucidate the photophysical process of 4,8-disubstituted benzobisthiazole derivatives, we also synthesized 2,6-didodecyl-4,8-diphenyl-benzo[1,2-*d*;4,5-*d*′]bisthiazole (**3**) and 2,6-didodecyl-4,8-dipyrrole-2-yl-benzo[1,2-*d*;4,5-*d*′]bisthiazole (**5**) using the Stille reaction, and investigated their structural and optical properties in solution and the solid state. Complementing the experimental study, density function theory (DFT) and ZINDO calculations were also performed to determine the configurations of molecular orbitals and transition probabilities for excited states based on optimized structures. The electronic structures of these 4,8-bisubstituted benzobisthiazole derivatives were clearly established, and a model for the absorbing and emitting levels was presented. This work has relevance in delineating correlations between molecular structure and observed photophysical properties of related 4,8-disubstituted benzobisthiazole derivatives.

CHART 1: Molecular Structures of 3a, 5a, and 6

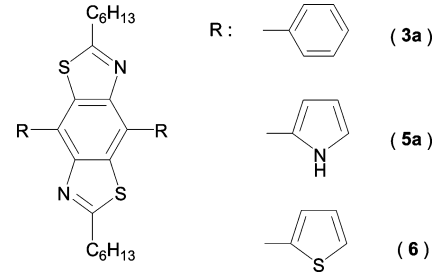

Experimental Section

Synthesis. ***Stille Reaction.*** All reactions were carried out in dry nitrogen. DMF was dried over CaH_2 and distilled just before use. ^{1}H NMR spectra were recorded on a 400 MHz JEOL instrument, and ^{13}C NMR spectra were recorded on a 100 MHz JEOL instrument. A solution of compound **1**[10] (0.002 mol) in dried DMF was purged with N_2 for 5 min and heated at 30−50 °C to yield a transparent solution. Compound **2** (0.0045 mol) and $Pd(PPh_3)_4$ (0.01 mmol) were added to the solution, and the mixture was stirred at room temperature for 5 min, heated quickly to 120 °C, and held at this temperature for 24 h. The progress of the reaction was monitored by thin layer chromatography(TLC) check and by observing color changes in the reaction mixture. After the reaction, the mixture was cooled to room temperature, and solvent was evaporated. The residue was dissolved in 100 mL of dichloromethane and washed with 100 mL of distilled water (five times). The organic layer was separated and dried over anhydrous magnesium sulfate. The solvent was evaporated, and the residue was separated on a

* Corresponding authors. Fax: +81-42-821-6548 (J.G.K.); +82-2-909-1978 (I.T.K.). E-mail: jgkang@cnu.ac.kr (J.G.K.); itkim@kw.ac.kr (I.T.K.).
† Chungnam National University.
‡ Kwangwoon University.

10.1021/jp912018h
Published on Web 02/26/2010

SCHEME 1

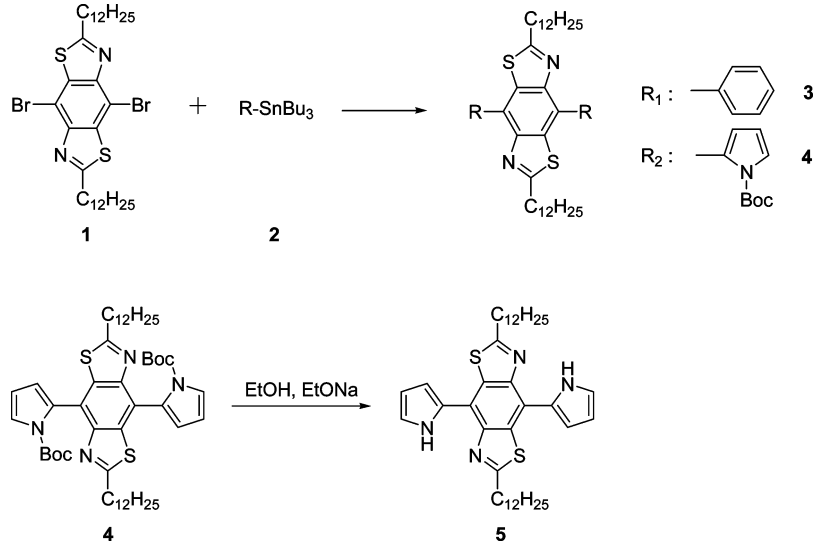

neutral silica gel column eluted with dichloromethane/hexane or ethyl acetate/hexane. In particular, we could only measure ^{1}H NMR spectrum of compound **4** because of its low stablility.

Compound **3** was obtained as a white solid in 82% yield. ^{1}H NMR ($CDCl_3$): δ 7.86−7.84 (m, 4H), 7.57−7.53 (m, 4H), 7.49−7.44 (m, 2H), 3.08−3.04 (t, 4H, J = 8.0 Hz), 1.85−1.78 (quin, 4H, J = 8.0 Hz), 1.41−1.24 (m, 36H), 0.89−0.85 (t, 6H, J = 8.0 Hz). ^{13}C NMR ($CDCl_3$): δ 172.81, 148.41, 138.62, 135.76, 129.77, 128.43, 128.24, 128.03, 34.69, 31.47, 29.59, 28.84, 22.49, 14.01. Anal. Found: C, 77.61; H, 9.02; N, 4.33; S 9.25. Calcd for $C_{44}H_{60}N_2S_2$: C, 77.58; H, 8.80; N, 4.11; S, 9.41. mp = 123 °C.

Compound **4** was obtained as a yellow solid in 60% yield. ^{1}H NMR ($CDCl_3$): δ 7.09−7.08 (d, 2H), 7.03−7.02 (t, 2H), 6.47−6.45 (d, 2H), 3.26−2.22 (t, 2H), 2.03−1.96 (m, 4H), 1.53−1.50 (s, 18H), 1.43−1.26 (m, 36H), 0.90−0.86 (t, 6H).

Removal of the Boc Group. Compound **4** (6.88 mmol) was dissolved in 50 mL of ethanol. A solution of freshly prepared sodium ethoxide (prepared by reacting 950 mg of Na (41 mmol) in 20 mL of ethanol) was added, and the reaction mixture was refluxed over 3 h. The solvent was evaporated, and the residue was treated with water (100 mL) and extracted with CH_2Cl_2 (50 mL). The organic extracts were dried over anhydrous $MgSO_4$, the solvent was evaporated, and the residue was purified on a silica gel column with a CH_2Cl_2/Hexane (1:9) eluent.

Compound **5** was obtained in 75% yield. ^{1}H NMR (DMSO): δ 7.01(s, 2H), 7.02−7.03 (d, 2H), 6.45−6.46 (s, 2H), 3.27−3.23 (t, 4H, J = 8.0 Hz), 2.03−1,96 (m, 4H, J = 8.0 Hz), 1.41−1.26 (m, 36H, J = 8.0 Hz), 0.89−0.86 (t, 6H, J = 8.0 Hz). ^{13}C NMR (DMSO): δ 172.11, 146.15, 129.24, 128.82, 119.60, 116.85, 109.72, 109.59, 34.38, 31.57, 29.49, 28.95, 28.88, 22.56, 14.07. Anal. Found: C, 73.18; H 9.06; N, 8.63; S, 9.47. Calcd for $C_{40}H_{58}N_4S_2$: C, 72.89; H, 8.80; N, 8.49; S, 9.72. mp = 135 °C (Scheme 1).

Optical Measurements. Absorption spectra of **3** and **5** dissolved in CH_2Cl_2 were recorded on a Hitach U-4100 UV−vis spectrophotometer. For luminescence and excitation spectra measurements, powdered samples were placed on the coldfinger of an Oxford CF-1104 cryostat using silicon grease. Excited light from either a He−Cd laser or an Oriel 1000 W Xe arc lamp passed through an Oriel MS257 monochromator and was focused on the sample. Luminescence and excitation spectra were measured at 90° relative to the excitation beam path with an ARC 0.5 m Czerny−Turner monochromator equipped with a cooled Hamamatsu R-933-14 photomultiplier tube. Solution phase spectra of each compound were dissolved in CH_2Cl_2 at a concentration of 5.0×10^{-4} M.

The relative quantum yield of the visible luminescence for each sample (Φ_s) was determined by a relative comparison against a reference of known quantum yield (quinine sulfate in diluted H_2SO_4 solution, $\Phi_r = 0.546$). The general equation used in the determination of relative quantum yield is given as follows:[11]

$$\Phi_s = \Phi_r\left(\frac{A_r(\lambda_r)}{A_s(\lambda_s)}\right)\left(\frac{I(\lambda_r)}{I(\lambda_s)}\right)\left(\frac{n_s^2}{n_r^2}\right)\left(\frac{D_s}{D_r}\right)$$

In the equation, $A(\lambda)$ is the absorbance, $I(\lambda)$ is the relative intensity of excitation light at wavelength λ, n is the average refractive index of the solvent, and D is the integrated area under the corrected emission spectrum. The recorded spectra for the quantum yield were corrected for the spectral response of the system using an Oriel 45 W quartz tungsten halogen lamp standard.

Molecular Modeling. 2,6-Hexyl-4,8-diphenyl-benzo[1,2-*d*;4,5-*d*′]bisthiazole (**3a**) and 2,6-hexyl-4,8-dipyrrole-2-yl-benzo[1,2-*d*;4,5-*d*′]bisthiazole (**5a**) (Chart 1) were chosen as model molecules for **3** and **5**, respectively, for the comparison with the X-ray crystallographic data for **6**. Molecular geometries were optimized at the DFT/B3LYP/6-31g(d,p) level using Gaussian 03.[12] On the basis of these optimized geometries, rotational barriers between the mainframe and the 2,6-substituted moiety were calculated by changing the dihedral angle between the two components. Configuration interaction singles (CIS) calculations were then performed to determine electronic structures and electronic transitions using semiempirical (ZINDO) method.

Results and Discussion

Absorption. Figure 1 shows the absorption spectra of **3** and **5** dissolved in CH_2Cl_2. The absorption spectrum of **3** exhibits three bands at 343, 309, and 276 nm. Hereafter, these bands are referred to as the A-, B-, and C-absorption bands, in order of increasing energy. The absorption spectra of dissolved hexyl-

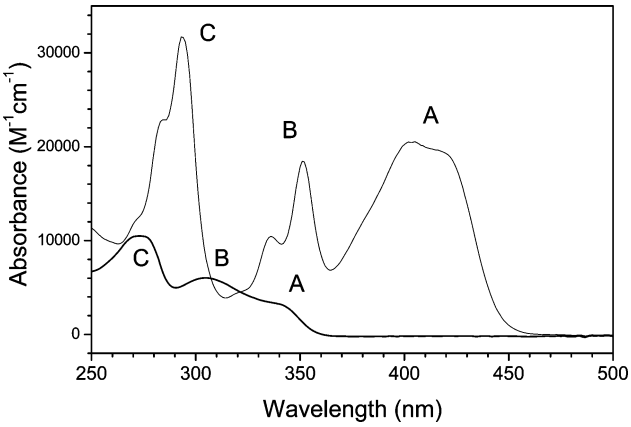

Figure 1. Absorption spectra of **3** (lower) and **5** (upper) dissolved in CH_2Cl_2.

substituted **3a** and **5a** were identical to those of **3** and **5**. The absorption spectrum of pyrrole-substituted **5** was very different from that of the phenyl-substituted **3**. For **5**, three characteristic absorption bands appear in the 250−450 nm region; hereafter, these bands are referred to as the A-, B- and C-absorption bands, in order of increasing energy. The A-absorption band, with a barycenter at 411 nm, was very broad and consisted of at least three Gaussian components with peaks at 425, 401, and 390 nm. The B-absorption comprised two components with peaks at 352 and 337 nm. The C-absorption, which peaked at 295 nm, was accompanied by two subpeaks at 285 and 275 nm. The band shape and the intensity of the C-band were very similar to that of thiophene-substituted **6**. The C-absorption can therefore be attributed to electronic transitions within the benzothiazole frame. These results indicate that the A-band of **5** is associated with the substituted pyrrole moiety.

Luminescence and Excitation. Photoluminescence (PL), excitation spectra, and the quantum yields of **3** and **5** were measured in CH_2Cl_2. As shown in Figure 2(a), the PL spectrum of **3** peaked at 404 nm and exhibited a narrow bandwidth with a full width at half-maximum (fwhm) of 2590 cm^{-1}. The excitation spectra of both the 400 and 420 nm emissions spanned over the 250−370 nm region. The peak position of the excitation spectrum (348 nm) coincided with that of the A-band. The Stokes' shift is approximately 4010 cm^{-1}. The narrow fwhm and the large Stokes' shift suggest that the emitting state may differ from the absorbing state. Figure 2b shows the PL and the excitation spectra of **5** dissolved in CH_2Cl_2. Compared with that of **3**, the PL spectrum of **5** was broad (fwhm = 3390 cm^{-1}) and exhibited a doublet structure consisting of a high-energy (HE) emission at 454 nm and a low-energy (LE) emission at 489 nm. The PL quantum yield of **5** (Φ = 14%) was much higher than that of **3** (Φ = 5%). We also measured the excitation spectra of the HE and LE emissions. The two excitation spectra differed slightly, as indicated in Figure 2b. The 450 nm excitation spectrum could be resolved into three characteristic regions: 370−440, 320−370, and 250−320 nm. The excitation spectrum of the HE emission resembled the absorption spectrum. The peak position of the excitation spectrum corresponds to the center of the A-band. However, the excitation spectrum of the LE emission (λ_{ems} = 510 nm) peaked at 460 nm.

The doublet structure of the A-band emission from **5** may be attributed to $\pi-\pi$ stacking of the benzobisthiazole frame and the pyrrole moieties to form a planar structure. The PL properties of **3** and **5** dissolved in CH_2Cl_2 as a function of concentration show that the spectral shape of **3** was invariant as a function of concentration. Conversely, the spectral shape

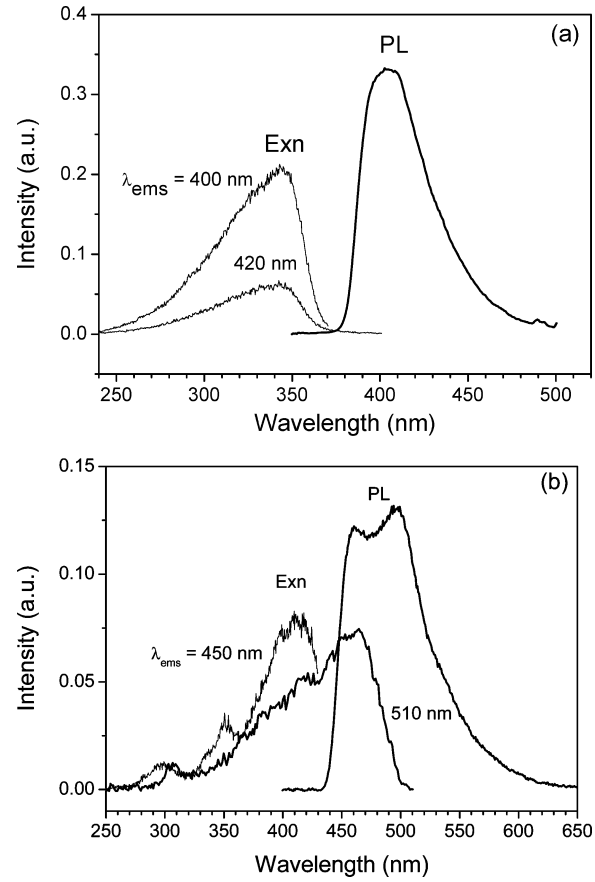

Figure 2. PL and excitation spectra of **3** (a) and **5** (b) dissolved in CH_2Cl_2 (5.0×10^{-4} M).

of **5** was very concentration dependent, as shown in Figure 3. The results for these band analyses are listed in Table S1 in the Supporting Information. At 5×10^{-6} M, the oscillator strength (OS) of the LE emission was almost 5 times larger than that of the HE emission. The OS of both the LE and the HE emissions increased gradually with concentration, and the ratio of the two emissions was approximately invariant up to 1×10^{-4} M. Above this concentration, the relative contribution of the HE emission increased markedly. The emission color-change response of 5 is visually described in Figure 4: a concentrated solution displayed a strong blue emission and a diluted solution emitted a strong green light under 366 nm UV light.

This contrasts with the anticipated effects of $\pi-\pi$ stacking, which typically enhances the degree of LE emission with increasing compound concentration. Concentration effects were also evaluated in CCl_4, (*cis*-CHCl)$_2$, and THF. Figure 3 shows that the concentration dependence of **5** in (*cis*-CHCl)$_2$ was very similar to that in CH_2Cl_2. In CCl_4 and THF, however, the HE and LE emissions were roughly equivalent at low concentration, and the intensity ratio of the two bands was almost independent of solution concentration. Solvent effects on luminescence properties have been well observed for intramolecular proton transfer (ESIPT) reactions, depending on the polarity of solvent.[13–16] Among the solvents evaluated, THF had the highest polarity, whereas CCl_4 was nonpolar. These results indicate that the observed solvent effects may be associated more with the partial charge of the hydrogen atom on the solvent molecule than with the polarity of the solvent. In both CH_2Cl_2 and (*cis*-CHCl)$_2$, the highly electronegative chlorine atom induces a partial positive charge on the hydrogen atom, whereas the partial charge of the hydrogen atom in THF is very low, and CCl_4 has no hydrogen atom.

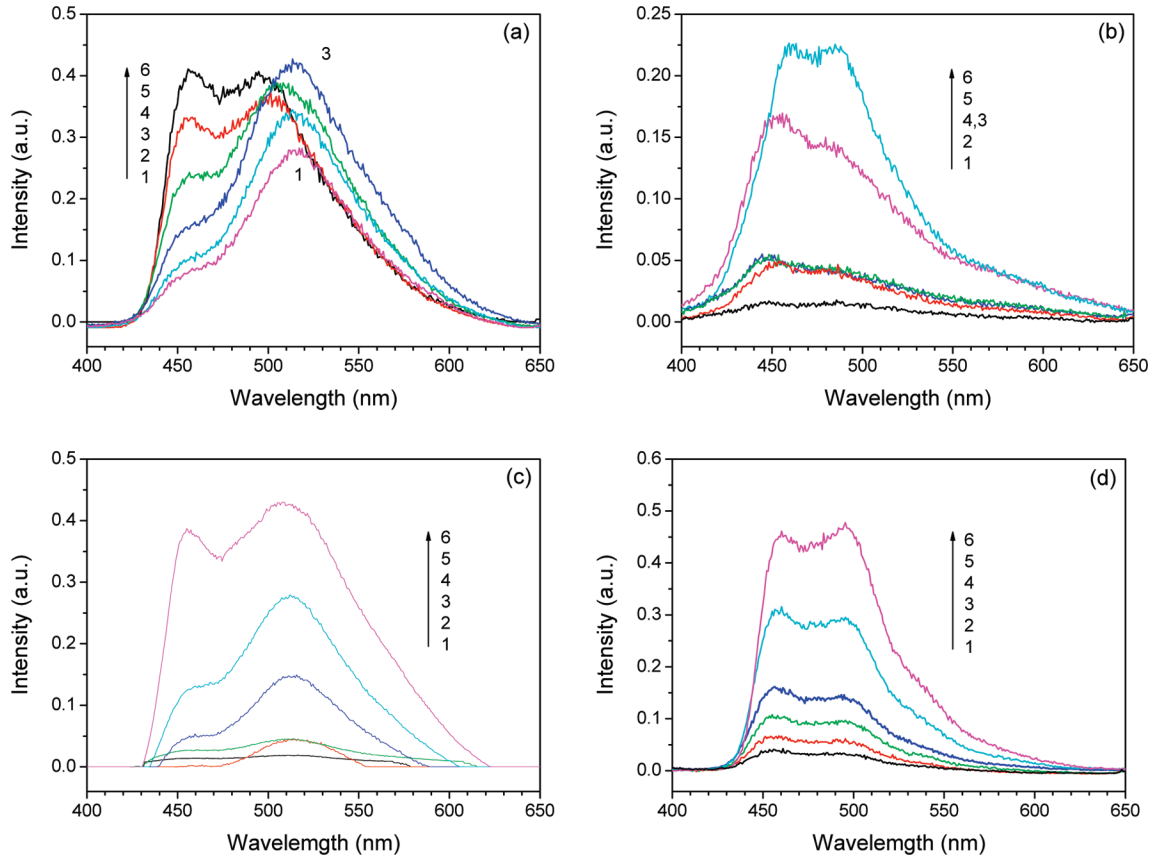

Figure 3. PL spectra of **5** in CH_2Cl_2 (a), CCl_4 (b), (*cis*-$CHCl)_2$ (c), and THF (d) at various concentrations (1. 5.0×10^{-6}, 2. 1.0×10^{-5}, 3. 5.0×10^{-5}, 4. 1.0×10^{-4}, 5. 5.0×10^{-4}, 6. 1.0×10^{-3} M.

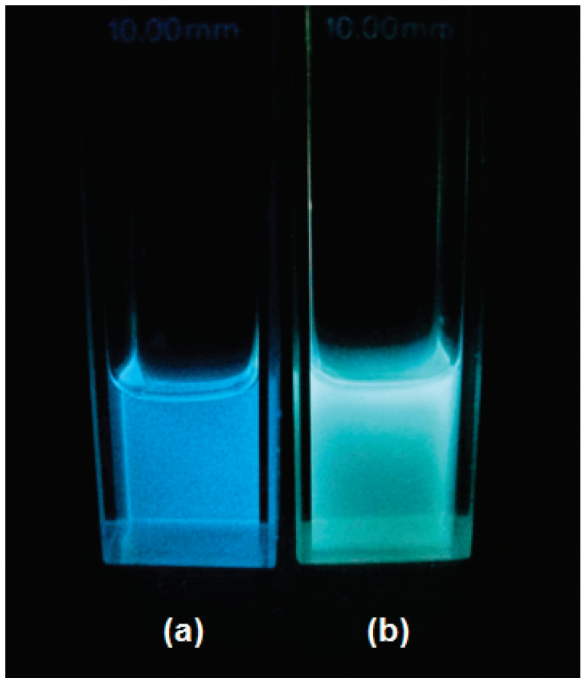

Figure 4. Digital photograph of CH_2Cl_2 solution of sample **5** under 366 nm UV lamp: (a) 1.0×10^{-3} M and (b) 5.0×10^{-6} M.

Compound **5** may adopt either a monomeric or oligomeric configuration in solution via the N−H···N intra- or intermolecular hydrogen bond formation, respectively, between the pyrrole moiety and the benzothiazole frame. Intramolecular hydrogen bonding in the monomer results in a planar geometry and allows π conjugation over the pyrrole moieties and the benzothiazole frame. In the oligomer, the pyrrole moiety may be twisted toward the benzothiazole frame to minimize the steric hindrance between the two adjacent frames. Solvents with no H atoms (CCl_4) or weakly charged H atoms (THF) do not affect hydrogen bonding. However, solvents such as CH_2Cl_2 and (*cis*-$CHCl)_2$, which contain highly electropositive H atoms, may form C−H···N hydrogen bonds between the solvent and the molecule **5**. At low concentrations, this could reduce the probability of oligomer formation. At high concentrations, the frequency of interactions between individual molecules of **5** increases, and the oligomeric configuration becomes more favorable. The doublet structure of the A-band emission from **5** in solution is attributed to the intramolecular and the intermolecular hydrogen bond formation appearing as the LE and the HE bands, respectively.

The luminescence spectra of **3** and **5** were also measured in the solid state at $T = 10$ K and room temperature (RT). Figure 5 shows that powdered **3**, when excited at 340 nm, produced a primary luminescence spanning from 350 to 540 nm, accompanied by a weak band from 540 to 650 nm. This weak band appeared only at low temperature. The overall shape of the solid-state spectra at RT was similar to that in solution. At 10 K, a vibronic distortion was evident in the solid state, with an average peak spacing of 1480 cm^{-1}. This suggests a vibronic distortion associated with the C−C stretching of the phenyl group. The excitation spectra of the 440 nm and the 560 nm emissions at 10 K are shown in Figure 5. Both spectra span from 250 to 420 nm, with a strong peak in the low-energy region. The high-energy excitation band between 250 and 360 nm was identical to the excitation spectrum obtained in solution. The low-energy peak, which was not observed in solution, overlaps with the emission spectrum. It suggests that the absorbing center responsible for the low-energy peak may be identical to the

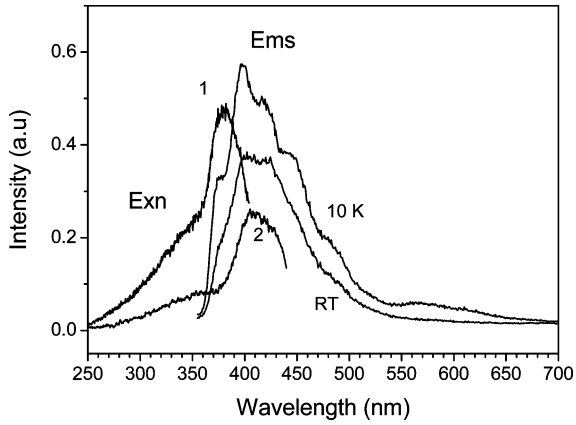

Figure 5. Emission and excitation spectra of **3** (Ems: $\lambda_{exn} = 340$ nm; Exn: $\lambda_{ems} = 1.440$, 2.560 nm at 10 K).

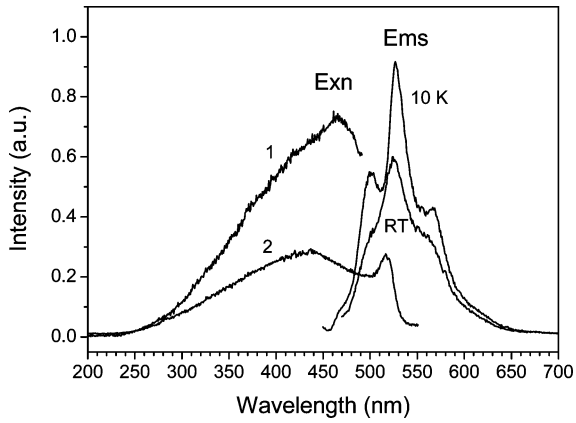

Figure 6. Emission and excitation spectra of **5** (Ems: $\lambda_{exn} = 380$ nm; Exn: $\lambda_{ems} = 1.520$ nm, 2.580 nm at 10 K).

emitting center. Furthermore, the excitation spectrum of the 560 nm emission shows that the low-energy emission between 540 and 650 nm is associated with the triplet state.

Figure 6 shows the luminescence spectra of powdered **5**, excited at 380 nm. As was the case for **3**, the low-temperature spectrum exhibits three well-resolved peaks at 500, 528, and 566 nm. The average spacing between these peaks in the solid-state spectrum was 1120 cm^{-1}, which is much narrower than the spacing (1655 cm^{-1}) between the corresponding doublet observed in emission from CH_2Cl_2 solution. A strong and unique vibrational band at 1120 cm^{-1} appears in the IR spectrum of **5**, which suggests that a multicomponent structure may arise from vibronic distortions by the pyrrole ring. With increasing temperature, the intensity of the luminescence and the degree of vibronic distortion decreased. Figure 6 also shows that at 10 K, the excitation spectrum of the 520 nm emission was very broad, with a peak at 434 nm. Although the peak position of this excitation band was almost the same as that observed in solution, the barycenter of the emission in the solid state was red-shifted by approximately 50 nm relative to that in solution. These results suggest that the observed emission from the solid state corresponds to the low-energy emission from the solution state, which would indicate that intrahydrogen bonding was predominant in the solid state. At 10 K, the excitation spectrum of the 580 nm emission exhibited a sharp peak at 516 nm, corresponding to the zero-phone transition, which can be correlated with the emission at 566 nm.

Structural Calculations and Assignments. Quantum mechanical calculations were performed to characterize the excited states and electronic transitions of **3** and **5**. Molecular geometries

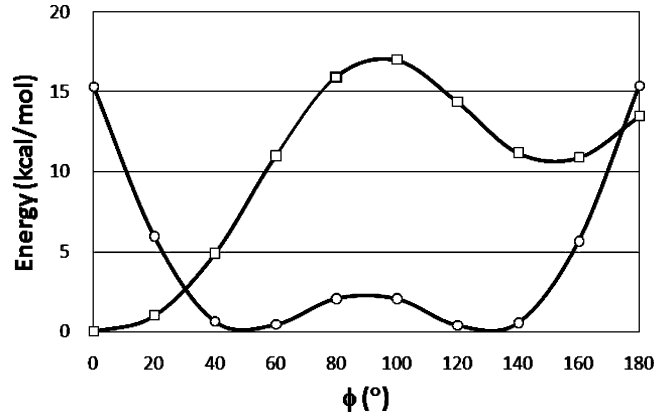

Figure 7. Rotational energy barrier between the center and two neighboring phenyl (square) and pyrrole (circle).

TABLE 1: Barycenter (nm) and Molar Absorbance of Absorption Bands Dissolved in CH_2Cl_2

compound	λ_{abs} ($\varepsilon/1 \times 10^4$, CH_2Cl_2)	assignment
3	343 (0.9)	$\pi \rightarrow \pi^*$ (bisbenzobisthiazole)
	309 (1.9)	$\pi \rightarrow \pi^*$ (bisbenzobisthiazole)
	276 (3.2)	$\pi \rightarrow \pi^*$ (bisbenzobisthiazole)
5	411 (3.6)	π (pyrrole) $\rightarrow \pi^*$ (bisbenzobisthiazole)
	352 (2.6)	$\pi \rightarrow \pi^*$ (bisbenzobisthiazole)
	337 (1.5)	$\pi \rightarrow \pi^*$ (bisbenzobisthiazole)
	295 (6.4)	π (pyrrole) $\rightarrow \pi^*$ (bisbenzobisthiazole)

were optimized at the level of DFT/B3LYP/6-31g(d,p). An Ortep view of **6** is shown in Figure S1 (Supporting Information), and optimized molecular geometries of **3a** and **5a** are shown in Figure S2 (Supporting Information). Selected geometric parameters and a comparison with empirical X-ray data of **6** are listed Table S2 (Supporting Information). The calculated values pertaining to the benzobisthiazole frames of **3a** and **5a** differ from those of **6** by less than 1%. The absorption and luminescence spectra of **3** and **5**, shown above, suggest that the 4,8-disubstituted phenyl or pyrrole moieties play a key role in determining the optical properties. The dihedral angles (ϕ) between the benzobisthiazole frame and the 4,8-disubstituted phenyl or pyrrole moieties determine the degree of π-orbital delocalization. Starting from the optimized conformations, ϕ between the benzobisthiazole frame and the substituted moiety on one side and $-\phi$ for the other part were rotated from 0° to 180° in 10° increments. As shown in Figure 7, these calculations indicate global minima of 50° for **3a** and 0° for **5a**. In **3a**, the substituted phenyl group is almost perpendicular to the mainframe, indicating that the steric hindrance within the molecule is unfavorable for a planar structure. In contrast, **5a** forms a planar structure with a high degree of electronic resonance. The combination of intrahydrogen bonding ($d_{NH\cdots H} = 2.250$ Å) between the NH group of the pyrrole and the nitrogen atom of the benzobisthiazole frame and the degree of π-resonance is sufficient to overcome unfavorable steric hindrances between the benzobisthiazole frame and the 4,8-disubstituted pyrrole moieties.

By use of the optimized geometries of the molecules **3a** and **5a**, the electronic structures and the electronic transitions were calculated at the level of ZINDO. The results of the molecular orbital (MO) calculations for **3a** are listed in Table 2. The two highest-occupied molecular orbitals (HOMOs), $h1$ and $h2$, were composed of a linear combination of the p_x and p_y orbitals of C atoms in the benzobisthiazole frame. Note that the molecular axis is represented by the z-axis. The contributions from the π-electron systems of the benzobisthiazole frame were 77 and 83%, respectively. The next three HOMOs, $h3-h5$, correspond

TABLE 2: Some DFT Molecular Orbitals Calculated for 3a

		main frame				
MO	hartree	8C	2N	2S	phenyl 12C	hexyl 12C
*l*12	0.099	68	0	19	13	0
*l*11	0.085	46	0	24	3	28
*l*10	0.081	41	3	20	0	30
*l*9	0.078	71	3	14	9	4
*l*8	0.067	73	25	0	2	0
*l*7	0.045	51	4	0	46	0
*l*6	0.033	23	14	0	63	0
*l*5	0.031	0	0	0	100	0
*l*4	0.030	0	0	0	100	0
*l*3	0.023	46	20	0	35	0
*l*2	0.011	70	0	0	30	0
*l*1	−0.007	91	9	0	0	0
*h*1	−0.273	77	9	0	14	0
*h*2	−0.294	83	0	8	9	0
*h*3	−0.318	6	0	0	94	0
*h*4	−0.329	0	0	0	100	0
*h*5	−0.330	0	0	0	100	0
*h*6	−0.337	24	8	12	56	0
*h*7	−0.377	17	55	6	8	0
*h*8	−0.383	25	58	4	0	0

TABLE 3: CIS Excited States and Predominant Transitions of 3a

excited state	nm	oscillator strength	predominant transition
1^1A_u	337	0.065	*h*1 → *l*2, *h*1, *h*2 → *l*1
2^1A_u	333	0.421	*h*1 → *l*1, *h*2 → *l*1
3^1A_u	292	0.941	*h*2 → *l*1, *h*1 → *l*2
4^1A_u	284	0.104	*h*7 → *l*1
5^1A_u	277	0.017	*h*1 → *l*5, *h*3 → *l*4
6^1A_u	257	0.462	*h*2 → *l*2
7^1A_u	241	0.033	*h*1 → *l*9,*l*7
8^1A_u	238	0.053	*h*1 → *l*9
9^1A_u	231	0.096	*h*1 → *l*7
10^1A_u	225	0.137	*h*2 → *l*9
11^1A_u	223	0.217	*h*1 → *l*5
12^1A_u	221	0.271	*h*1 → *l*8
13^1A_u	215	0.103	*h*6 → *l*1, *h*1, *h*2 → *l*8
14^1A_u	210	0.270	*h*2 → *l*5, *h*6 → *l*1
15^1A_u	208	0.331	*h*2 → *l*7, *h*2 → *l*5, *h*1 → *l*8
16^1A_u	206	0.238	*h*6 → *l*2

to the π-orbitals of the phenyl groups with a contribution of more than 94%. The lowest unoccupied molecular orbital (LUMO), *l*1, is the π-antibonding orbital of the carbon atoms in the benzobisthiazole frame with a minor contribution from nitrogen atoms. The contribution of the carbon atoms in the benzobisthiazole frame is 91%. The next two LUMOs, *l*2 and *l*3, comprise contributions from both the benzobisthiazole frame and the phenyl groups. The contribution of the phenyl groups to *l*2 and *l*3 is less than 35%. The next two LUMOs, *l*4 and *l*5, correspond to the π-antibonding orbitals of the phenyl groups.

The calculated low-lying excited states and oscillator strengths of **3a** are listed in Table 3. Note that excitations from the X ground state to all A_g excited states are forbidden under C_i symmetry. Those transitions were excluded from Table 3. According to the energy gap and the oscillator strength, the excited states can be classified into three groups. The first two A_u states were classified into group A and predominantly arise from the *h*1 → *l*2 and the *h*1 → *l*1 transitions, respectively. The X → $1A_u$ transition with $f = 0.065$ is weak, whereas the X → $2A_u$ transition with $f = 0.421$ is predominant. The X → $2A_u$ transition is likely the main contributor to the A-band in the absorption spectrum. Accordingly, the A-band can be attributed to the $\pi \rightarrow \pi^*$ transition of the benzobisthiazole frame. The

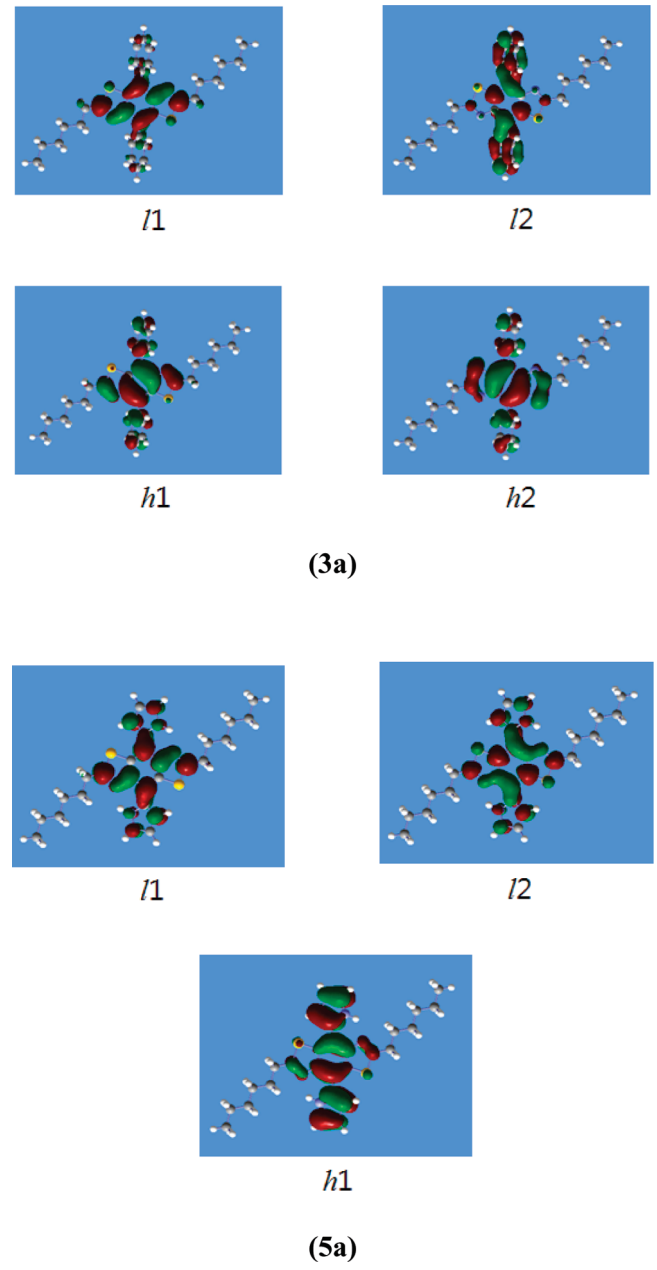

Figure 8. Contour plots of the molecular orbitals for **3a** and **5a** involved in the A-band excitation and emission.

next three A_u states, $3A_u$−$5A_u$, can be included in group B. The $3A_u$ excited state occurs predominantly from the *h*2 → *l*1 and *h*1 → *l*2 transitions. The X → $3A_u$ transition exhibited the largest calculated oscillator strength, $f = 0.941$ and can be attributed to the B-band in the absorption spectrum. Table 3 shows several close-lying excited states. Among these, the X → $6A_u$ transition has the largest transition probability with $f = 0.462$. The $6A_u$ excited state arises predominantly from the *h*2 → *l*2 transition. Therefore, the C-band in the absorption spectrum is composed primarily of the $\pi \rightarrow \pi^*$ transition of the benzobisthiazole frame. The predominant orbital transitions involved in the A-band excitation and emission are represented in Figure 8, and the assignments of the absorption bands of **3** are listed in Table 1.

A characteristic feature of the A-band emission from **3** in solution is that the excitation spectrum does not overlap with the emission spectrum. The large Stokes' shift of 4010 cm^{-1} suggests that the absorbing and the emitting centers differ. A

TABLE 4: Some DFT Molecular Orbitals Calculated for 5a

		main frame			pyrrole		hexyl
MO	hartree	8C	2N	2S	8C	2N	12C
*l*11	0.097	19	0	0	82	0	0
*l*10	0.084	5	0	0	95	0	0
*l*9	0.083	45	3	21	3	0	28
*l*8	0.078	42	0	20	0	0	32
*l*7	0.075	73	0	14	8	0	5
*l*6	0.070	29	4	0	62	5	0
*l*5	0.055	65	21	0	12	2	0
*l*4	0.047	11	7	0	68	13	0
*l*3	0.019	66	26	3	5	0	0
*l*2	0.007	79	3	3	12	3	0
*l*1	−0.017	79	4	0	15	3	0
*h*1	−0.245	36	0	0	64	0	0
*h*2	−0.286	7	0	0	93	0	0
*h*3	−0.291	94	4	2	0	0	0
*h*4	−0.337	3	0	0	68	29	0
*h*5	−0.339	0	0	0	63	37	0
*h*6	−0.349	25	8	22	30	13	0
*h*7	−0.369	12	79	9	0	0	0
*h*8	−0.374	11	77	9	0	3	0
*h*9	−0.396	25	49	26	0	0	0

possible pathway is as follows: the 2^1A_u excited state gains population through the A-band excitation and then transitions nonradiatively from the 2^1A_u state to the 1^1A_u. The observed blue emission then occurs from the 1^1A_u state. In the solid state, the A-band emission from 1^1A_u state is achieved through direct excitation mainly. Consequently, the overlap between the excitation and the emission spectra is very large and results in the phosphorescence at the low temperature via intersystem crossing to the 1^3A_u state.

The MO contributions of **5a** are listed in Table 4. The *h*1 HOMO is composed of π-orbitals from the benzobisthiazole frame and the pyrrole rings. The contribution of the two pyrrole rings (64%) is much higher than that of the benzobisthiazole frame (36%). The orbital nature of *h*1 of **5a** is significantly different from that of **3a**. The next two HOMOs, *h*2 and *h*3, correspond to the π-bonding orbitals of the pyrrole moieties and the benzobisthiazole frame, respectively. The first two LUMOs, *l*1 and *l*2, arise from the linear combinations of the p_x and p_y orbitals of carbon atoms in the benzobisthiazole frame, with a contribution of 79% each. The compositions of these two orbitals of **5a** are similar to those of **3a**. Selected excited states and the oscillator strengths of **5a** are listed in Table 5. According to the energy gaps and the oscillator strengths, the $1A_u-2A_u$, $3A_u-4A_u$, and $5A_u-9A_u$ excited states are responsible for the A-, B-, and C-bands, respectively. In group A, the two excited states arise from the transitions from the *h*1 HOMO to the *l*1 and *l*2 LUMOs and are associated with the transition from the π-system of the pyrrole rings to the π^*-system of the benzobisthiazole frame, respectively. The $X \rightarrow 1A_u$ transition has a large oscillator strength, with $f = 0.802$. The π (pyrrole moieties) $\rightarrow \pi^*$ (benzobisthiazole) transitions may be responsible for the A-band and are observed as a doublet with a strong intensity in the low-energy region compared with the $\pi \rightarrow \pi^*$ transitions of the benzobisthiazole frame as observed with **3**. These transitions are made feasible by the planar structure of **5**. The $X \rightarrow 3A_u$ and $4A_u$ transitions can be attributed the B1- and B2-bands, respectively. The $3A_u$ and $4A_u$ excited states arise from the *h*3 $\rightarrow$ *l*1 and the *h*8 $\rightarrow$ *l*3 transitions, respectively. Accordingly, the B1- and B2-bands are associated with the $\pi \rightarrow \pi^*$ transitions of the benzobisthiazole frame. The transitions in the C group may be classified into the $X \rightarrow 5A_u$, and the $X \rightarrow 7A_u$ and $8A_u$ transitions. The predominance of these transitions indicates that these excited states are associated with the $\pi \rightarrow \pi^*$ transitions of the benzobisthiazole frame and the π (pyrrole moieties) $\rightarrow \pi^*$ (benzobisthiazole) transitions, respectively. Accordingly, the C-band can be assigned as the combination of these two characters. The predominant orbital transitions involved in the A-band excitation and emission from **5a** are represented in Figure 8, and the assignments of the absorption bands are listed in Table 1. The 1^1A_u excited state is responsible for the absorbing and emitting center. Emission from **5** is predominantly produced via A-band excitation.

TABLE 5: CIS Excited States and Predominant Transitions of 5a

excited state	nm	oscillator strength	predominant trans.
1^1A_u	401	0.802	*h*1 → *l*1
2^1A_u	370	0.098	*h*1 → *l*2
3^1A_u	321	0.841	*h*3 → *l*1
4^1A_u	293	0.012	*h*8 → *l*3, *h*7 → *l*1
5^1A_u	278	0.101	*h*3 → *l*2
6^1A_u,	261	0.0	*h*1 → *l*7
7^1A_u	258	0.021	*h*1 → *l*5,*l*6
8^1A_u	249	0.058	*h*1 → *l*5,*l*6
9^1A_u	245	0.019	*h*2 → *l*3
10^1A_u	230	0.01	*h*3 → *l*7
11^1A_u	228	0.126	*h*6 → *l*1, *h*1 → *l*6,*l*11
12^1A_u	217	0.006	*h*2 → *l*3, *h*3 → *l*5
13^1A_u	216	0.001	*h*1 → *l*9
14^1A_u	215	0.695	*h*6 → *l*1, *h*4 → *l*1
15^1A_u	212	0.229	*h*6 → *l*1, *h*1 → *l*11, *h*4 → *l*1
16^1A_u	209	0.015	*h*1 → *l*9

Conclusion

The effects of π-electron-rich substituents on the optical properties of benzobisthiazole derivatives 2,6-didodecyl-4,8-diphenyl-benzo[1,2-*d*;4,5-*d*′]bisthiazole (**3**) and 2,6-didodecyl-4,8-dipyrrole-2-yl-benzo[1,2-*d*;4,5-*d*′]bisthiazole (**5**) were evaluated. DFT quantum mechanical calculations indicate that the dihedral angle between the substituted ring and the benzobisthiazole frame is approximately 50° and 0° for phenyl and pyrrole substituents, respectively. Due to its nonplanar structure, the HOMO and LUMO levels of **3** are composed entirely of the π-character from the benzobisthiazole frame. The observed blue luminescence is strongly associated with these two orbitals. The planar structure of **5** allows the π-character of HOMO to expand over all of the carbon atoms in the pyrrole rings, constituting a 64% contribution, and over the benzobisthiazole frame, for the remaining 36% contribution. The observed greenish yellow luminescence of powdered **5** is strongly associated with the electronic transitions between the pyrrole ring and the benzobisthiazole frame.

Acknowledgment. This research was supported by National Research Foundation (2009-0073199). J.-G.K. and Y.-K.J. acknowledge the fellowships of the BK 21 program. Y.J.B., S.W.L., and I.T.K. acknowledge the technology development project of new and renewable energies of the Ministry of Knowledge Economy of the Republic of Korea and a research grant of Kwangwoon University (2009).

Supporting Information Available: Ortep view (Figure S1) and optimized (Figure S2), and concentration dependence of oscillator strengths of the emission bands (Table S1) and comparison of geometric parameters from optimization calculation (Table S2). This material is available free of charge via the Internet at http://pubs.acs.org.

References and Notes

(1) Tan, L.-S.; Burkett, J. L.; Simko, S. R.; Alexander, M. D., Jr. *Macromol. Rapid Commun.* **1999**, *20*, 16.

(2) Dudis, D. S.; McKellar, B. R. *Polym. Prepr.* **2000**, *41*, 235.

(3) Tan, L.-S.; Simko, S. R.; Bai, A. J.; Vaia, R. A.; Taylor, B. E.; Houtz, M. D.; Alexander, M. D., Jr.; Spry, R. J. *J. Polym. Sci., B: Polym. Phys.* **2001**, *39*, 2539.

(4) Pang, H.; Vilela, F.; Skabara, P. J.; McDouall, J. J. W.; Crouch, D. J.; Anthopoulos, T. D.; Bradley, D. D. C.; de Leeuw, D. M.; Horton, P. N.; Hursthouse, M. B. *Adv. Mater.* **2007**, *19*, 4438.

(5) Fedorov, Y. V.; Fedorova, O.; Schepel, N.; Alfimov, M.; Turek, A. M.; Saltiel, J. *J. Phys. Chem. A* **2005**, *109*, 8653.

(6) Baek, J.-B.; Lyons, C. B.; Tan, L.-S. *J. Mater. Chem.* **2009**, *19*, 4172.

(7) Zhang, X.; Jenekhe, S. A. *Macromolecules* **2000**, *33*, 2069.

(8) Kawamoto, T.; Takeda, K.; Nishiwaki, M.; Aridomi, T.; Konno, T. *Inorg. Chem.* **2007**, *46*, 4239.

(9) Kang, J.-G.; Cho, H.-G.; Kang, S. K.; Park, C.; Lee, S. W.; Park, G. B.; Lee, J. S.; Kim, I. T. *J. Photochem. Photobiol. A: Chem.* **2006**, *183*, 212.

(10) Kim, I. T.; Lee, S. W.; Kim, S. Y.; Lee, J, S,; Park, G. B.; Lee, S. H.; Kang, S. K.; Kang, J.-G.; Park, C.; Jin, S.-H. *Synth. Met.* **2006**, *156*, 38.

(11) Demas, J. N.; Crosby, G. A. *J. Phys. Chem.* **1971**, *75*, 991.

(12) Frisch, M. J. ; Trucks, G. W.; Schlegel, H. B.; Scuseria, G. E.; Robb, M. A.; Cheeseman, J. R.; Montgomery Jr., J. A.; Vreven, T.; Kudin, K. N.; Burant, J. C.; Millam, J. M.; Iyengar, S. S.; Tomasi, J.; Barone, V.; Mennucci, B.; Cossi, M.; Scalmani, G.; Rega, N.; Petersson, G. A.; Nakatsuji, H.; Hada, M.; Ehara, M.; Toyota, K.; Fukuda, R.; Hasegawa, J.; Ishida, M.; Nakajima, T.; Honda, Y.; Kitao, O.; Nakai, H.; Klene, M.; Li, X.; Knox, J. E.; Hratchian, H. P.; Cross, J. B.; Bakken, V.; Adamo, C.; Jaramillo, J.; Gomperts, R.; Stratmann, R. E.; Yazyev, O.; Austin, A. J.; Cammi, R.; Pomelli, C.; Ochterski, J. W.; Ayala, P. Y.; Morokuma, K.; Voth, G. A.; Salvador, P.; Dannenberg, J. J.; Zakrzewski, V. G.; Dapprich, S.; Daniels, A. D.; Strain, M. C.; Farkas, O.; Malick, D. K.; Rabuck, A. D.; Raghavachari, K.; Foresman, J. B.; Ortiz, J. V.; Cui, Q.; Baboulv, A. G.; Clifford, S.; Cioslowski, J.; Stefanov, B. B.; Liu, G.; Liashenko, A.; Piskorz, P.; Komaromi, I.; Martin, R. L.; Fox, D. J.; Keith, T.; Al-Laham, M. A.; Peng, C. Y.; Nanayakkara, A.; Challacombe, M.; Gill, P. M. W.; Johnson, B.; Chen, W.; Wong, M. W.; Gonzalez, C.; Pople, J. A. *Gaussian 03, Revision C.02*; Gaussian, Inc.: Wallingford, CT, 2004.

(13) Wang, R.; Liub, D.; Xua, K.; Li, J. *J. Photochem. Photobiol. A: Chem.* **2009**, *205*, 61.

(14) Mandal, P. K.; Samanta, A. *J. Phys. Chem. A* **2003**, *107*, 6334.

(15) Henary, M. M.; Fahrni, C. J. *J. Phys. Chem. A* **2002**, *106*, 5210.

(16) Sun, W.; Li, S.; Hu, R.; Qian, Y.; Wang, S.; Yang, G. *J. Phys. Chem. A* **2009**, *113*, 5888.

JP912018H